

SuperCarver: Texture-Consistent 3D Geometry Super-Resolution for High-Fidelity Surface Detail Generation

Qijian Zhang^{1†}, Xiaozheng Jian¹, Xuan Zhang¹, Wenping Wang², Junhui Hou³

¹Tencent Games ²Texas A&M University ³City University of Hong Kong

{keeganzhang, ajian, libzhang}@tencent.com

wenping@tamu.edu jh.hou@cityu.edu.hk



Figure 1. Given a 3D textured model lacking geometric details as input, **SuperCarver** generates realistic and expressive 3D surface details consistent with its texture appearance within 1 ~ 2 minutes, significantly enhancing the production efficiency of high-quality mesh assets. (Row 1: The input 3D textured meshes. Rows 2&4: The original coarse surfaces and normal maps. Rows 3&5: The resulting high-fidelity mesh surfaces and normal maps after our geometry super-resolution.)

Abstract

Traditional production workflow of high-precision 3D mesh assets necessitates a cumbersome and laborious process of

manual sculpting by specialized modelers. The recent years have witnessed remarkable advances in AI-empowered 3D content creation. However, although the latest state-of-the-arts are already capable of generating plausible structures and intricate appearances from images or text prompts, the actual mesh surfaces are typically over-smoothing and lack

[†] Corresponding author.

geometric details. This paper introduces SuperCarver, a 3D geometry super-resolution framework particularly tailored for adding texture-consistent surface details to given coarse meshes. Technically, we start by rendering the original textured mesh into the image domain from multiple viewpoints. To achieve geometric detail generation, we develop a deterministic prior-guided normal diffusion model fine-tuned on a carefully curated dataset of paired low-poly and high-poly normal renderings. To optimize mesh structures from potentially imperfect normal map predictions, we design a simple yet effective noise-resistant inverse rendering scheme based on distance field deformation. Extensive experiments show that SuperCarver generates realistic and expressive surface details as depicted by specific texture appearances, making it a powerful tool for automatically upgrading massive outdated low-quality assets and shortening the iteration cycle of high-quality mesh production in practical applications.

1. Introduction

3D modeling plays a key role in industrial design and digital entertainment fields, such as movies, video games, robotics, and virtual/augmented reality. In practice, the accuracy and quality of 3D mesh models directly influence specific downstream performances. However, creating high-quality mesh assets depends heavily on the manual efforts of specialized 3D modelers, which can be cumbersome and laborious.

Generally, the complete industrial 3D modeling pipeline can be broadly divided into three sequential stages in terms of the geometric complexity of the corresponding mesh surface: **1)** Given initial concept designs, e.g., 2D sketch drawings, a *mid-poly* mesh is established to roughly replicate the overall spatial structure. **2)** Subsequently, surface sculpting is performed to produce highly expressive surface details on a *high-poly* mesh, which typically consists of million-scale faces. **3)** To ensure the efficiency of the rendering engine, a *low-poly* mesh with significantly simplified faces is created based on the high-poly mesh, followed by UV unwrapping, detail (such as normal/bump map) baking, and texture painting. Among the above procedures, the effects of high-poly geometry sculpting greatly determine the ultimate graphics quality and visual realism, but it accounts for a large portion of the entire manual workload. Therefore, there is an urgent need to particularly investigate the automated generation of high-fidelity surface details.

The recent advancements of deep learning-based generative modeling have led to remarkable strides in 3D content generation [51]. Restricted by insufficient 3D training data, early zero-shot architectures such as DreamFields [37] and DreamFusion [78] resort to distilling prior knowledge from pre-trained vision-language multi-modal models [84] or 2D image diffusion models [87]. However, such per-shape optimization process can typically suffer from inefficiency and

inter-view inconsistency problems. Since the emergence of large-scale mesh datasets [22, 23], feed-forward 3D generation frameworks such as LRM [35] and InstantMesh [117] have received increasing attention, which can achieve end-to-end training and finish inference within several seconds. To further enhance generation quality without significantly compromising efficiency, another family of research such as SyncDreamer [58], Wonder3D [59], and Unique3D [113] proposes to apply multi-view diffusion models to synthesize 2D novel views and then reconstruct the target 3D mesh via iterative optimization procedures. In addition, analogous to 2D image diffusion, native 3D latent diffusion architectures such as CLAY [127] also demonstrate tremendous potential. Overall, the current state-of-the-art 3D generation methods are already capable of producing plausible geometric structures and intricate texture appearances. However, the actual mesh surfaces tend to be over-smoothing and lack geometric details, as shown in Figure 2. Moreover, it is worth noting that existing 3D generation approaches are designed for creating new 3D assets from fundamental creative elements, i.e., reasoning the underlying 3D structures from 2D images or text prompts. This means that they cannot be directly applied on a given 3D model for further enhancement, because there is no guarantee that the original structural characteristics could still be well preserved. In addition to image/text-to-3D generation paradigms, there also exist several lines of relevant studies, such as point cloud upsampling [81, 123], reference-based [10, 33] or text-guided [29, 85] 3D editing, geometric (e.g., depth/normal) map [2, 27, 41] or PBR material [104, 107] estimation. However, there is still a lack of specialized explorations for enhancing the surface details of specifically given 3D models.

In this paper, we present SuperCarver, a novel geometry super-resolution framework operating on a given 3D model for generating realistic and expressive surface details as depicted by its texture appearance. Considering the difficulties of directly learning 3D structural details, we choose normal maps, a 2.5D representation format, to efficiently bridge 2D and 3D domains. Accordingly, we start by rendering the input textured mesh into image space, which facilitates leveraging the power and pre-trained knowledge of image diffusion architectures. Still, accurately and robustly predicting normal maps through diffusion faces several challenges. On the one hand, normals are a form of sensitive and vulnerable geometric property, i.e., moderate numerical variations can lead to obvious damage to the underlying surface. Besides, without sufficient priors, normals predicted in image space often fail to align with the actual surface structures of given meshes. On the other hand, due to the inherent stochasticity of diffusion models, it is inevitable that normal predictions vary across different inferences. To address these problems, inspired by previous attempts to stabilize [45, 116] and accelerate [108, 124] image diffusion mechanisms, we adopt

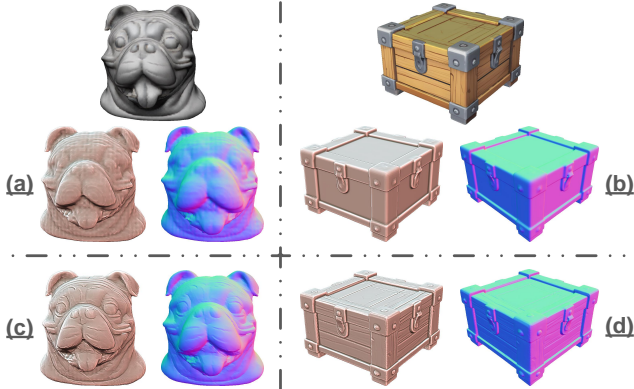


Figure 2. The generation results of the current state-of-the-arts, (a) InstantMesh [117] & (b) CLAY [127], typically lack high-fidelity surface details. The corresponding geometry enhancement results of our proposed SuperCarver are shown in (c) & (d).

a chain of deterministic interpolations from rendered coarse normal maps to desired high-precision normal maps. In the meantime, necessary conditioning signals are incorporated by extracting semantic and geometric priors from rendered color images and depth maps.

After enhancing normal maps from multiple viewpoints, it is straightforward to perform gradient-based mesh updating [43]. Since optimizing from potentially imperfect multi-view predicted normal maps is prone to causing severe surface degradation, we customize a simple yet effective noise-resistant inverse rendering approach based on distance field deformation to deduce the corresponding surface details.

We conduct comprehensive performance evaluations and comparisons on a manually selected subset of textured mesh models from Objaverse [23] and ABO [21] datasets, which strongly demonstrate the effectiveness of our approach. We also verify that SuperCarver can be applied on off-the-shelf image/text-to-3D frameworks to further enhance the geometry quality of their generation results.

2. Related Work

2.1. 3D Content Generation

3D content generation [51, 54, 93] has always been a highly valuable yet rather challenging task. Unfortunately, the limited data volume and diversity of classic 3D shape repositories [8, 115] largely restrict the advancement of this field. In order to bypass the reliance on large-scale 3D training data, zero-shot schemes [37, 69, 71] are designed to constrain the text-prompted 3D generation process using the off-the-shelf language-image prior of CLIP [84]. With the advent of pre-trained 2D image diffusion models [34, 87, 95], score distillation [53, 68, 78, 105] is investigated to inject text guidance into the optimization procedure of various neural field representations [42, 70]. Subsequent researches further make continuous progress in improving generation quality and/or speed [11, 19, 49, 62, 83, 100, 110, 120], enabling 3D edit-

ing [85, 97], and supplementing image conditioning capabilities [66, 80, 92, 98]. Nevertheless, the distillation-based generation paradigm necessitates sophisticated processing to deal with inefficiency and inter-view inconsistency.

Thanks to the significant increase in the scale of 3D data [22, 23], it becomes promising to directly train feed-forward 3D generation networks. The pioneering work of LRM [35] builds an end-to-end regression framework to predict a tri-plane [7] NeRF representation, while Instant3D [46] develops a two-stage framework that begins with generating the “view-compiled” image grid from texts. Numerous follow-up studies continue to improve performances from different perspectives [103], such as shifting to the 3DGS [42] representation (LGM [99]), replacing transformers with convolutional architectures (CRM [111]), and adding more geometric supervisions (InstantMesh [117]).

To further boost the generation quality while maintaining satisfactory efficiency, viewpoint-conditioned 2D diffusion [55, 56] is explored to synthesize novel 2D views, followed by iterative optimization for sparse-view 3D reconstruction. However, lifting imperfect multi-view 2D predictions to 3D can be non-trivial and usually problematic. To ensure multi-view consistency, SyncDreamer [58] designs synchronized multi-view noise prediction by constructing an intermediate 3D feature volume. In Zero123++ [91], multiple images are tiled into a single frame to model the joint distribution of all pre-defined views. Wonder3D [59] builds a new multi-view cross-domain 2D diffusion pipeline controlled by a domain switcher to generate multi-view normal maps and color images, after which explicit 3D geometry is extracted via normal fusion. Era3D [47] incorporates explicit regression of camera parameters and designs more efficient and compact multi-view attention. Unique3D [113] constructs a powerful image-to-3D framework with comprehensive improvements in multi-view generation and upscaling of color images and normal maps, together with an efficient multi-stage mesh reconstruction algorithm.

Analogous to 2D diffusion for image generation, another promising direction is to develop native 3D diffusion architectures [44, 50, 114, 125, 127] for conditional 3D generation with different design choices of latent space representations. Additionally, auto-regressive generation of triangle sequences [12, 15, 94, 101, 112] and UV-domain diffusion [26, 118] driven by regular geometry image representations [30, 128, 129] also demonstrate new potential.

2.2. Inverse Rendering and Mesh Optimization

Inverse rendering aims at reasoning the underlying physical attributes of a target 3D scene from its 2D image observations. Different 3D scene parameters such as geometry, texture, material, and lighting can be optimized via backpropagating the gradients w.r.t. the 2D rendering outputs [32, 72]. Earlier research investigates various differentiable renderers

[13, 40, 57, 60]. Later studies [5, 6, 38, 96, 126, 130] devote to learning neural field representations. For gradient-based mesh optimization, the most straightforward way is to explicitly perform surface deformation from pre-defined mesh templates [31, 106]. Nevertheless, directly optimizing the mesh vertex positions is prone to surface defect and degeneracy, thus requiring careful initialization, regularization, and remeshing [73, 76]. Another choice is to employ occupancy and distance fields [13, 67, 77] for implicit surface modeling. Since traditional iso-surface extraction algorithms [25, 39, 61, 74] cannot propagate gradients, various differentiable schemes [16, 18] are designed to operate on discrete occupancy grids (DMC [52]), continuous signed distance fields (MeshSDF [86]), or deformable tetrahedrons (DefTet [28], DM Tet [89]). Moreover, NJF [1] depicts the mappings between pairs of source and target triangles via Jacobian matrices. FlexiCubes [90] incorporates carefully-chosen learnable parameters into [74] for achieving much more flexible local adjustment of mesh vertices.

2.3. 3D Geometry Enhancement

Instead of directly generating textured meshes from images or text prompts, another line of research aims to enhance the geometric surface of given 3D models.

Similar to image super-resolution [109], point cloud up-sampling [48, 65, 79, 81, 82, 121, 123, 129] can produce a denser set of spatial points uniformly located on the underlying 3D surface from sparse and possibly noisy inputs. However, these approaches are rarely capable of generating new geometric details. When a high-quality source mesh is given as the reference, detail transfer [4, 33] can synthesize similar geometric patterns on the target surface. More recent works [9, 10, 17] further apply such an exemplar-based paradigm on coarse voxels for few-shot 3D shape detailization. Text-guided mesh editing frameworks [3, 19, 29] facilitate flexible and convenient geometry manipulation, but face challenges in accurate and fine-grained control. Additionally, PBR material generation [14, 104, 107, 122] typically involves estimating normal/bump maps, which can be potentially exploited for refinement purposes.

3. Proposed Method

3.1. Overall Workflow

Given a 3D textured model \mathcal{M} with vertices \mathcal{V} and faces \mathcal{F} , we aim at generating high-fidelity surface details to produce the updated geometric mesh structure $\mathcal{M}^u = (\mathcal{V}^u, \mathcal{F}^u)$. As illustrated in Figure 3, we start by rendering \mathcal{M} from certain specified viewpoint to obtain the corresponding color image $\mathcal{I} \in \mathbb{R}^{H \times W \times 3}$, normal map $\mathcal{N} \in \mathbb{R}^{H \times W \times 3}$, and depth map $\mathcal{D} \in \mathbb{R}^{H \times W}$. We achieve geometry super-resolution with a two-stage pipeline. In the first stage, we construct a deterministic prior-guided 2D diffusion architecture to predict a

high-precision normal map $\mathcal{H} \in \mathbb{R}^{H \times W \times 3}$. By performing inferences from multiple different viewpoints, we can acquire a set of multi-view normal map predictions $\{\mathcal{H}_k\}_{k=1}^K$. In the second stage, we design a noise-resistant inverse normal rendering approach to iteratively optimize the original mesh surface with geometric constraints, where we perform distance field deformation by learning grid offsets. In what follows, we will detail the two stages.

3.2. Deterministic Prior-Guided Normal Diffusion

We resort to the most popular text-to-image latent diffusion architecture [87] to leverage its strong generalization power and adapt it to generate texture-consistent detail-rich normal maps. Some previous studies [58, 59, 91, 113] resort to joint multi-view diffusion to mitigate inconsistency across views. Still, such a modeling paradigm also restricts the flexibility in adjusting the number and positions of viewpoints if users have personalized needs to designate specific surface areas for geometric detail carving, which are common in practical scenarios. Moreover, since in our setting there is no need to infer invisible novel views from limited visual observations, inter-view inconsistency will not be a major problem. Thus, we choose the more flexible single-view working mode.

To achieve this goal, the most straightforward solution is to denoise the noisy latent representation of the target normal map \mathcal{H} while incorporating the color image \mathcal{I} into the denoising U-Net. Thus, the forward process is given by:

$$\tilde{\mathcal{H}}_t = \sqrt{\bar{\alpha}_t} \cdot \tilde{\mathcal{H}} + \sqrt{1 - \bar{\alpha}_t} \cdot \epsilon, \quad t = \{1, \dots, T\}, \quad (1)$$

where the noise schedule term $\bar{\alpha}_t$ controls the transformation to the standard Gaussian distribution ϵ , T is the number of time steps, $\tilde{\mathcal{H}}$ denotes the latent representation of \mathcal{H} after VAE’s encoder, and $\tilde{\mathcal{H}}_t$ is the noisy feature map.

Given the denoising network μ_θ , the optimization objective can be formulated as:

$$\mathcal{L}_\theta = \mathbb{E}_{\epsilon, \tilde{\mathcal{I}}, \tilde{\mathcal{H}}, \mathbf{c}, t} [\|\epsilon - \mu_\theta(\tilde{\mathcal{I}}, \tilde{\mathcal{H}}_t, \mathbf{c}, t)\|_2^2], \quad (2)$$

where \mathbf{c} is a vectorized embedding originally extracted from texts. The visual cues can be injected via concatenating $\tilde{\mathcal{H}}_t$ with the encoded latent feature map (denoted as $\tilde{\mathcal{I}}$) of \mathcal{I} .

Deterministic Diffusion. In fact, the above implementation together with various existing approaches [27, 59, 113] can be regarded as cross-domain (RGB2Normal) image translation, while our special setting motivates us to directly refine the rendered coarse normal map \mathcal{N} to generate the desired high-precision normal map \mathcal{H} . To this end, we investigate a deterministic diffusion mechanism, whose forward process can be formulated as:

$$\tilde{\mathcal{H}}_t = \sqrt{\bar{\alpha}_t} \cdot \tilde{\mathcal{H}} + \sqrt{1 - \bar{\alpha}_t} \cdot \tilde{\mathcal{N}}, \quad t = \{1, \dots, T\}, \quad (3)$$

where we directly replace the Gaussian noise ϵ (in Eq. (1)) with the latent representation $\tilde{\mathcal{N}}$ of the rendered normal map \mathcal{N} after VAE’s encoder.

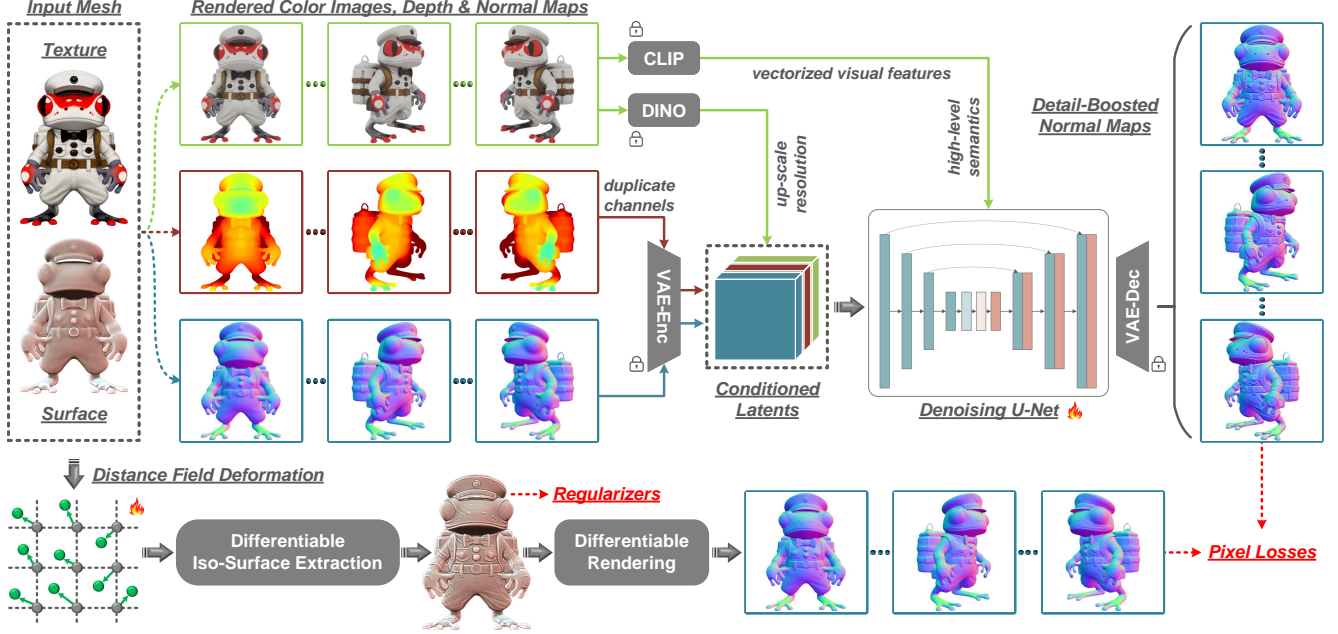


Figure 3. The overall workflow of our proposed SuperCarver for texture-consistent geometry super-resolution. Given an input 3D textured model, we start by rendering color, depth, and normal maps, which are fed into a customized deterministic prior-guided diffusion architecture to generate detail-boosted normal maps. To perform gradient-based mesh refinement from potentially imperfect multi-view normal map predictions, we design a noise-resistant distance field deformation process to drive the optimization of high-fidelity 3D surface details.

Empirically, eliminating the inherent stochastic nature in this way naturally ensures deterministic outputs and avoids the fluctuations of diffused normal maps across views, thus implicitly enhancing inter-view consistency and stabilizing the subsequent multi-view inverse rendering process.

Prior Extraction. To boost the accuracy and robustness of normal diffusion, we further extract semantic and geometric priors as conditioning signals.

For the rendered color image \mathcal{I} , we extract its DINO [75] feature \tilde{Q} and also obtain its latent representation $\tilde{\mathcal{I}}$ through VAE’s encoder. The spatial resolution of \tilde{Q} is pre-upscaled by several auxiliary convolutional layers. Besides, we apply CLIP’s image encoder to extract the vectorized embedding \tilde{c} for cross-attention within U-Net’s transformer blocks. For the rendered depth map \mathcal{D} , we treat its latent representation $\tilde{\mathcal{D}}$ as the geometric prior. Then we concatenate \tilde{Q} , $\tilde{\mathcal{I}}$, and $\tilde{\mathcal{D}}$ to deduce the resulting conditioning signal $\tilde{\mathcal{S}}$.

Thus, we can achieve prior-guided diffusion by concatenating $\tilde{\mathcal{S}}$ with the noisy latent representation $\tilde{\mathcal{H}}_t$. The corresponding optimization objective can be formulated as:

$$\mathcal{L}_\theta = \mathbb{E}_{\tilde{\mathcal{N}}, \tilde{\mathcal{S}}, \tilde{\mathcal{H}}_t, \tilde{c}, t} [\|\tilde{\mathcal{N}} - \mu_\theta(\tilde{\mathcal{S}}, \tilde{\mathcal{H}}_t, \tilde{c}, t)\|_2^2]. \quad (4)$$

Empirically, we introduce another parameterization form of v-prediction [88] to train the denoising U-Net, whose input channels and cross-attention dimensions are adapted to match with our prior-conditioned latent representations and CLIP-encoded image embeddings.

3.3. Noise-Resistant Inverse Normal Rendering

When finishing the training of our normal diffusion model, we can render multi-view images from different viewpoints $\{\mathbf{v}_k\}_{k=1}^K$, and perform inference to correspondingly predict a set of detail-rich normal maps $\{\mathcal{H}_k \in \mathbb{R}^{H \times W \times 3}\}_{k=1}^K$.

To transfer the underlying 3D structural patterns implied by the predicted 2D normal maps to the input mesh surface, the common practice is to perform gradient-based mesh refinement through inverse rendering. However, it is observed that updating the mesh geometry from *potentially imperfect* normal map predictions is prone to causing obvious surface degradation, even with adaptations of various existing state-of-the-art (explicit [76] or implicit [90]) mesh optimization approaches. Hence, we are strongly motivated to develop a highly noise-resistant scheme better suited to our setting of adding new details to a given coarse surface.

We introduce a simple yet effective distance field deformation approach, working in a “value-fixing, grid-moving” manner. Specifically, assuming that the original mesh $\mathcal{M} = (\mathcal{V}, \mathcal{F})$ has already been normalized into the unit sphere, we start by constructing uniform 3D grid points $\mathcal{G} \in \mathbb{R}^{r \times r \times r \times 3}$ within $[-1, 1]^3$ and computing per-grid signed distance values $\mathcal{X} \in \mathbb{R}^{r \times r \times r}$. Different from common ways of implementing deformable distance field representations via only updating \mathcal{X} or jointly updating \mathcal{G} and \mathcal{X} , we choose a subtle strategy that fixes distance values \mathcal{X} while separately learning zero-initialized offsets $\mathcal{O} \in \mathbb{R}^{r \times r \times r \times 3}$ to move initial grid positions \mathcal{G} . In comparison, standard distance field refinement requires higher resolutions of fixed uniform grids;



Figure 4. Illustration of applying our proposed SuperCarver for further 3D surface detail generation on textured meshes generated from (a) InstantMesh [117], (b) Unique3D [113], and (c) CLAY [127].

otherwise, detailed structures cannot be captured even with accurate distance values. Additionally, fixing pre-computed distance values hinders the optimization process from drastically changing the original mesh structure even with obviously erroneous normal prediction in certain areas.

To achieve this, we employ a differentiable implementation of a classic iso-surface extraction algorithm DMC [74], which we denote as $\Psi(\cdot; \cdot)$, for producing an updated mesh $\mathcal{M}^u = (\mathcal{V}^u, \mathcal{F}^u)$. Then, a differentiable rasterizer $\mathcal{R}(\cdot; \cdot)$ is integrated to render the correspondingly updated normal maps $\{\mathcal{H}_k^u \in \mathbb{R}^{H \times W \times 3}\}_{k=1}^K$ w.r.t. every viewpoint \mathbf{v}_k . The whole processing procedure can be formulated as:

$$\mathcal{G}^u = \mathcal{G} + \tau \cdot \sigma(\mathcal{O}), \quad (5)$$

$$\mathcal{H}_k^u = \mathcal{R}(\Psi(\mathcal{G}^u; \mathcal{X}); \mathbf{v}_k), \quad (6)$$

where we bound the range of grid offset values by applying the hyperbolic tangent (Tanh) function $\sigma(\cdot)$ multiplied by a

positive scalar τ , then the deformed grid points \mathcal{G}^u and fixed distance values \mathcal{X} are used for the subsequent differentiable normal map rendering.

We iteratively optimize the grid offsets \mathcal{O} by minimizing the following objective function:

$$\min_{\mathcal{O}} \sum_{k=1}^K \|\mathcal{H}_k^u - \mathcal{H}_k\|_2^2 + \omega_s \cdot \mathcal{L}_s + \omega_n \cdot \mathcal{L}_n, \quad (7)$$

where the first term aligns every pair of diffusion-predicted and mesh-rendered normal maps, the last two terms denote mesh vertex and normal regularizations weighted by factors ω_s and ω_n . For each vertex \mathbf{p}_i in the updated mesh and its neighboring vertices $\Omega_i = \{\mathbf{p}_{i,j}\}$, the Laplacian smoothing is computed by:

$$\mathcal{L}_s = \sum_{\mathbf{p}_i \in \mathcal{V}^u} \sum_{\mathbf{p}_{i,j} \in \Omega_i} (\mathbf{p}_i - \mathbf{p}_{i,j}) / |\Omega_i|, \quad (8)$$

where $|\Omega_i|$ is the number of neighbors. Moreover, for each pair of neighboring normal vectors \mathbf{n}_i and \mathbf{n}_i' , we constrain

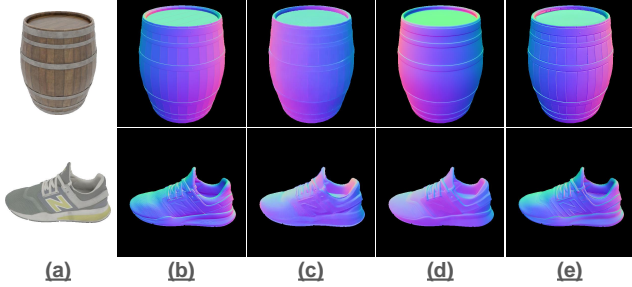


Figure 5. Visual comparison of normal map prediction results exported from (c) GeoWizard [27], (d) StableNormal [119], and (e) Ours, where (a) and (b) show the corresponding color images and ground-truth high-fidelity normal maps.

Table 1. Quantitative comparison of normal map prediction accuracy under the metric of mean angular error (MAE).

Method	GeoWizard [27]	StableNormal [119]	Ours
MAE ↓	17.59°	14.33°	9.05°

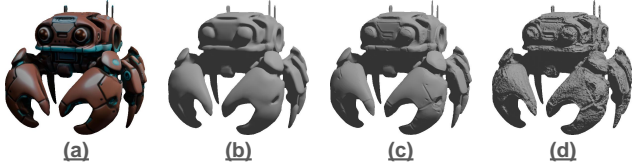


Figure 6. The rendering effects of (c) our optimized mesh and (d) attaching the bump map obtained from PBRBoost [76], given the input textured coarse mesh as presented in (a) and (b).

local orientation consistency by:

$$\mathcal{L}_n = \sum_i 1 - (\mathbf{n}_i \cdot \mathbf{n}'_i) / (\|\mathbf{n}_i\| \cdot \|\mathbf{n}'_i\|). \quad (9)$$

After iterative optimization, we moderately apply Taubin smoothing [102] as post-processing to mitigate meaningless surface wrinkles.

4. Experiments

Training Dataset Preparation. We used the publicly available Objaverse [23] dataset comprising 800K+ 3D assets to produce our training data. Through a series of meticulously designed filtering protocols and cleaning procedures, we ultimately acquired around 80K high-quality mesh models.

We used BlenderProc [24] for the rendering of color images, depth maps, and normal maps based on perspective projection. For each training mesh, we randomly sampled 16 viewpoints, with azimuth and elevation angles respectively varying within $[0^\circ, 360^\circ]$ and $[-30^\circ, 30^\circ]$.

To create paired low-poly and high-poly normal renderings, we performed geometry simplification on each high-poly training mesh model based on manifold reconstruction [36], and further removed detailed structures using [102]. We also manually annotated a smaller portion of unqualified training samples, which were used for training a separate neural model to further purify the whole training set.

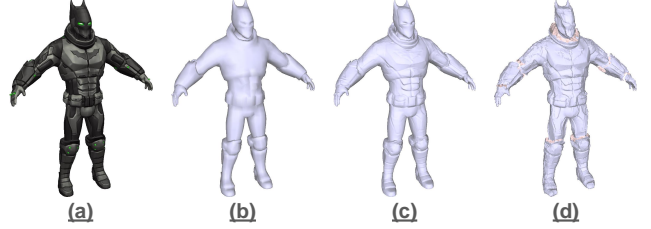


Figure 7. Comparison of mesh optimization effects, where (a) and (b) denote the input textured mesh, (c) and (d) present the results of our distance field deformation scheme and CR [76].

Table 2. Normal diffusion accuracy of different baseline schemes. *Stoc.* denotes the straightforward implementation of stochastic diffusion. *w/o Sem.* and *w/o Geo.* respectively denote removing the high-level semantics and low-level depth priors.

Method	Original	<i>Stoc.</i>	<i>w/o Sem.</i>	<i>w/o Geo.</i>
MAE ↓	9.05°	21.64°	10.49°	9.81°

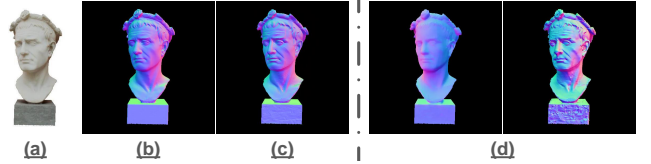


Figure 8. Illustration of prediction variation issues of the stochastic baseline diffusion scheme as displayed in (d). The color image, ground-truth normal map, and the output of our original design are presented in (a), (b), and (c).

Implementation Details. We adopted the popular diffusion architecture of Stable Diffusion V2.1 [87] and performed fine-tuning on 16 NVIDIA Tesla V100 GPUs for 40K steps with a total batch size of 128. We applied the AdamW [63] optimizer with cosine annealing, reducing the learning rate from $5e-5$ to $1e-5$. For both training and inference, the image resolution is configured to 512×512 .

For iterative mesh sculpting, we adopted Nvdiffrast [43] for efficient differentiable rendering from 12 camera poses (8 evenly-spaced horizontal views with azimuth angles from 0° to 360° and 4 downward-looking (elevated by 30°) views with azimuth angles $[45^\circ, 135^\circ, 225^\circ, 315^\circ]$). Camera intrinsics were kept the same as our configurations in BlenderProc. The hyperparameters were empirically tuned as $r = 512$, $\tau = 0.5$, $\omega_s = 0.25$, $\omega_n = 0.01$ for 200 iterations.

4.1. Performance Evaluation

Considering the lack of specialized research on our targeted task of texture-consistent 3D geometry super-resolution, we evaluated our superiority via applying SuperCarver on the textured meshes generated by various existing state-of-the-art 3D generation approaches, including InstantMesh [117], Unique3D [113], and CLAY [127], covering representative generation paradigms of feed-forward large reconstruction models, multi-view diffusion models, and native 3D latent diffusion models. As demonstrated in Figure 4, various input meshes are effectively boosted by our approach to pro-

duce realistic and expressive 3D surface details well aligned with the corresponding texture appearances.

Comparison on Normal Prediction. To evaluate the effectiveness of our specialized normal diffusion architecture, we made comparisons with advanced normal prediction frameworks, including GeoWizard [27] and StableNormal [119]. To facilitate quantitative evaluations, we manually selected 50 detail-rich textured meshes as ground-truths from Objaverse [23] and ABO [21] datasets. Then we applied surface simplification and smoothing to create geometrically-coarse meshes as the inputs.

As shown in Figure 5, our normal map predictions show better details and avoid obviously erroneous areas. Besides, we further deduced the metric of mean angular error (MAE) between ground-truth and predicted normal maps, where we masked invalid backgrounds for the outputs of GeoWizard and StableNormal. As illustrated in Table 1, owing to our specialized diffusion architecture, our normal map predictions significantly outperform the competing approaches. In addition, we also considered PBRBoost [107] (a latest material generation framework), since one of its outputs is the 2D bump maps associated with the base meshes, enabling us to compare its rendering effects when attaching the bump maps as height information. As shown in Figure 6, the actual fidelity of the enhanced geometric cues from PBRBoost is still far from satisfactory.

Comparison on Mesh Optimization. To facilitate surface geometry updating, many recent 3D generation frameworks [20, 50, 64, 113] introduce the CR [76] algorithm with joint optimization and remeshing, which is regarded as the most relevant competitor. In fact, we had previously attempted to adapt FlexiCubes [90], an advanced iso-surface representation, to achieve gradient-based geometry refinement starting from the initially given mesh surface. However, through extensive attempts, we empirically found that it easily leads to severe surface damages. We reason that this is attributable to its significantly increased deformation flexibility (which should have been its major strength) amplifies the impact of erroneous normal pixels. As shown in Figure 7, for typical hard cases with less accurate normal predictions, CR tends to produce noisy and degraded surfaces.

4.2. Ablation Study

To evaluate the effectiveness and necessity of the core components in our entire workflow, we conducted ablation study with different baseline schemes. We began with a straightforward baseline normal diffusion framework as formulated in Eq. (1) and Eq. (2). Besides, since prior guidance is also a critical condition for generating robust and accurate normal maps, we can design another two variants via removing the semantic cues extracted from DINO features or the geometric cues extracted from depth maps. As reported in Table 2, directly fine-tuning a standard diffusion model conditioned

Table 3. Quantitative comparison of different distance field deformation schemes. *Only Grids* means our original design, *Only Dist.* and *Joint G&D* are the corresponding two baseline variants.

Method	<i>Only Grids</i>	<i>Only Dist.</i>	<i>Joint G&D</i>
MAE ↓	4.22°	4.75°	5.47°

on color images lead to significantly degraded performance, with the MAE metric of 21.64°. More importantly, as illustrated in Figure 8, the stochastic nature inevitably results in unstable predictions. As reported in the last two columns of Table 2, the joint injection of semantic and geometric priors are indeed beneficial. In the inverse normal rendering stage, we experimented with another two distance field deformation schemes, i.e., fixing grids while optimizing distances; jointly updating grids and distances. To obtain quantitative results, we computed the MAE metric of normal maps *rendered* from optimized meshes (note that Table 1 and Table 2 are targeted at *diffused* normal maps). As evidenced in Table 3, the two variants show sub-optimal performances, in that only optimizing distances usually causes weakened details while the joint optimization strategy easily suffers from surface distortion especially when the diffused normal maps contain relatively larger errors.

5. Conclusion

This paper presents a specialized geometry super-resolution framework for generating high-fidelity 3D surface details as depicted in the texture appearances of given coarse meshes, serving as a powerful tool for automated surface sculpting. Our framework is normal-centric and consists of two stages. The first stage predicts view-specific detail-boosted normal maps through a deterministic prior-guided diffusion architecture. The second stage transfers the underlying geometric patterns on multi-view normal map predictions onto the original mesh surface through a noise-resistant inverse rendering scheme driven by a carefully designed distance field deformation mechanism. Experiments demonstrate the superior performance of our SuperCarver across various shape types and texture styles. We believe that our exploration can make a difference to significantly accelerate the creation of high-poly meshes, and inspire more focused research in 3D geometry super-resolution, which is highly valuable yet basically ignored in the current community.

Limitations & Future Works. Our current framework still struggles to handle *elongated* objects (e.g., knives, swords) because the rendered areas are too small to provide adequate appearance information under finite image resolutions. One straightforward solution is to apply localized sculpting procedures. Besides, the inherent properties of signed distance field representations restrict our capabilities to handle open surfaces and complicated topologies. Hence, we might need to introduce differentiable iso-surface extractors built upon more generic implicit geometry representations.

References

- [1] Noam Aigerman, Kunal Gupta, Vladimir G Kim, Siddhartha Chaudhuri, Jun Saito, and Thibault Groueix. Neural jacobian fields: Learning intrinsic mappings of arbitrary meshes. *ACM Trans. Graph.*, 41(4):1–17, 2022. 4
- [2] Gwangbin Bae and Andrew J Davison. Rethinking inductive biases for surface normal estimation. In *Proc. CVPR*, pages 9535–9545, 2024. 2
- [3] Amir Barda, Vladimir Kim, Noam Aigerman, Amit Haim Bermano, and Thibault Groueix. Magicclay: Sculpting meshes with generative neural fields. In *Proc. SIGGRAPH Asia*, pages 1–10, 2024. 4
- [4] Sema Berkiten, Maciej Halber, Justin Solomon, Chongyang Ma, Hao Li, and Szymon Rusinkiewicz. Learning detail transfer based on geometric features. In *Comput. Graph. Forum*, pages 361–373, 2017. 4
- [5] Mark Boss, Raphael Braun, Varun Jampani, Jonathan T Barron, Ce Liu, and Hendrik Lensch. Nerd: Neural reflectance decomposition from image collections. In *Proc. ICCV*, pages 12684–12694, 2021. 4
- [6] Mark Boss, Varun Jampani, Raphael Braun, Ce Liu, Jonathan Barron, and Hendrik Lensch. Neural-pil: Neural pre-integrated lighting for reflectance decomposition. *Proc. NeurIPS*, 34:10691–10704, 2021. 4
- [7] Eric R Chan, Connor Z Lin, Matthew A Chan, Koki Nagano, Boxiao Pan, Shalini De Mello, Orazio Gallo, Leonidas J Guibas, Jonathan Tremblay, Sameh Khamis, et al. Efficient geometry-aware 3d generative adversarial networks. In *Proc. CVPR*, pages 16123–16133, 2022. 3
- [8] Angel X Chang, Thomas Funkhouser, Leonidas Guibas, Pat Hanrahan, Qixing Huang, Zimo Li, Silvio Savarese, Manolis Savva, Shuran Song, Hao Su, et al. Shapenet: An information-rich 3d model repository. *arXiv preprint arXiv:1512.03012*, 2015. 3
- [9] Qimin Chen, Zhiqin Chen, Hang Zhou, and Hao Zhang. Shaddr: Interactive example-based geometry and texture generation via 3d shape detailization and differentiable rendering. In *Proc. SIGGRAPH Asia*, pages 1–11, 2023. 4
- [10] Qimin Chen, Zhiqin Chen, Vladimir G Kim, Noam Aigerman, Hao Zhang, and Siddhartha Chaudhuri. Decollage: 3d detailization by controllable, localized, and learned geometry enhancement. In *Proc. ECCV*, pages 110–127, 2024. 2, 4
- [11] Rui Chen, Yongwei Chen, Ningxin Jiao, and Kui Jia. Fantasia3d: Disentangling geometry and appearance for high-quality text-to-3d content creation. In *Proc. ICCV*, pages 22246–22256, 2023. 3
- [12] Sijin Chen, Xin Chen, Anqi Pang, Xianfang Zeng, Wei Cheng, Yijun Fu, Fukun Yin, Zhibin Wang, Jingyi Yu, Gang Yu, BIN FU, and Tao Chen. Meshxl: Neural coordinate field for generative 3d foundation models. In *Proc. NeurIPS*, 2024. 3
- [13] Wenzheng Chen, Huan Ling, Jun Gao, Edward Smith, Jaakko Lehtinen, Alec Jacobson, and Sanja Fidler. Learning to predict 3d objects with an interpolation-based differentiable renderer. In *Proc. NeurIPS*, pages 9609–9619, 2019. 4
- [14] Yongwei Chen, Rui Chen, Jiabao Lei, Yabin Zhang, and Kui Jia. Tango: Text-driven photorealistic and robust 3d stylization via lighting decomposition. In *Proc. NeurIPS*, pages 30923–30936, 2022. 4
- [15] Yiwen Chen, Tong He, Di Huang, Weicai Ye, Sijin Chen, Ji-axiang Tang, Zhongang Cai, Lei Yang, Gang Yu, Guosheng Lin, and Chi Zhang. Meshanything: Artist-created mesh generation with autoregressive transformers. In *Proc. ICLR*, 2025. 3
- [16] Zhiqin Chen and Hao Zhang. Neural marching cubes. *ACM Trans. Graph.*, 40(6):1–15, 2021. 4
- [17] Zhiqin Chen, Vladimir G Kim, Matthew Fisher, Noam Aigerman, Hao Zhang, and Siddhartha Chaudhuri. Decoran: 3d shape detailization by conditional refinement. In *Proc. CVPR*, pages 15740–15749, 2021. 4
- [18] Zhiqin Chen, Andrea Tagliasacchi, Thomas Funkhouser, and Hao Zhang. Neural dual contouring. *ACM Trans. Graph.*, 41(4):1–13, 2022. 4
- [19] Zilong Chen, Feng Wang, Yikai Wang, and Huaping Liu. Text-to-3d using gaussian splatting. In *Proc. CVPR*, pages 21401–21412, 2024. 3, 4
- [20] Jaehoon Choi, Rajvi Shah, Qinbo Li, Yipeng Wang, Ayush Saraf, Changil Kim, Jia-Bin Huang, Dinesh Manocha, Suhub Alsisan, and Johannes Kopf. Ltm: Lightweight textured mesh extraction and refinement of large unbounded scenes for efficient storage and real-time rendering. In *Proc. CVPR*, pages 5053–5063, 2024. 8
- [21] Jasmine Collins, Shubham Goel, Kenan Deng, Achleshwar Luthra, Leon Xu, Erhan Gundogdu, Xi Zhang, Tomas F Yago Vicente, Thomas Dideriksen, Himanshu Arora, et al. Abo: Dataset and benchmarks for real-world 3d object understanding. In *Proc. CVPR*, pages 21126–21136, 2022. 3, 8
- [22] Matt Deitke, Ruoshi Liu, Matthew Wallingford, Huong Ngo, Oscar Michel, Aditya Kusupati, Alan Fan, Christian Laforte, Vikram Voleti, Samir Yitzhak Gadre, Eli VanderBilt, Aniruddha Kembhavi, Carl Vondrick, Georgia Gkioxari, Kiana Ehsani, Ludwig Schmidt, and Ali Farhadi. Objaverse-xl: A universe of 10m+ 3d objects. In *Proc. NeurIPS*, 2023. 2, 3
- [23] Matt Deitke, Dustin Schwenk, Jordi Salvador, Luca Weihs, Oscar Michel, Eli VanderBilt, Ludwig Schmidt, Kiana Ehsani, Aniruddha Kembhavi, and Ali Farhadi. Objaverse: A universe of annotated 3d objects. In *Proc. CVPR*, pages 13142–13153, 2023. 2, 3, 7, 8
- [24] Maximilian Denninger, Dominik Winkelbauer, Martin Sundermeyer, Wout Boerdijk, Markus Knauer, Klaus H. Strobl, Matthias Humt, and Rudolph Triebel. Blenderproc2: A procedural pipeline for photorealistic rendering. *J. Open Source Softw.* 7
- [25] Akio Doi and Akio Koide. An efficient method of triangulating equi-valued surfaces by using tetrahedral cells. *IE-ICE Trans. Inf. Syst.*, 74(1):214–224, 1991. 4
- [26] Slava Elizarov, Ciara Rowles, and Simon Donn e. Geometry image diffusion: Fast and data-efficient text-to-3d with image-based surface representation. In *Proc. ICLR*, 2025. 3

- [27] Xiao Fu, Wei Yin, Mu Hu, Kaixuan Wang, Yuexin Ma, Ping Tan, Shaojie Shen, Dahua Lin, and Xiaoxiao Long. Geowizard: Unleashing the diffusion priors for 3d geometry estimation from a single image. In *Proc. ECCV*, pages 241–258, 2024. 2, 4, 7, 8
- [28] Jun Gao, Wenzheng Chen, Tommy Xiang, Alec Jacobson, Morgan McGuire, and Sanja Fidler. Learning deformable tetrahedral meshes for 3d reconstruction. In *Proc. NeurIPS*, pages 9936–9947, 2020. 4
- [29] William Gao, Noam Aigerman, Thibault Groueix, Vova Kim, and Rana Hanocka. Textdeformer: Geometry manipulation using text guidance. In *Proc. SIGGRAPH*, pages 1–11, 2023. 2, 4
- [30] Xianfeng Gu, Steven J Gortler, and Hugues Hoppe. Geometry images. *Proc. SIGGRAPH*, 21(3):355–361, 2002. 3
- [31] Rana Hanocka, Gal Metzer, Raja Giryes, and Daniel Cohen-Or. Point2mesh: A self-prior for deformable meshes. *ACM Trans. Graph.*, 39(4):1–12, 2020. 4
- [32] Jon Hasselgren, Nikolai Hofmann, and Jacob Munkberg. Shape, light, and material decomposition from images using monte carlo rendering and denoising. In *Proc. NeurIPS*, pages 22856–22869, 2022. 3
- [33] Amir Hertz, Rana Hanocka, Raja Giryes, and Daniel Cohen-Or. Deep geometric texture synthesis. *ACM Trans. Graph.*, 39(4):108:1–108:11, 2020. 2, 4
- [34] Jonathan Ho, Ajay Jain, and Pieter Abbeel. Denoising diffusion probabilistic models. In *Proc. NeurIPS*, pages 6840–6851, 2020. 3
- [35] Yicong Hong, Kai Zhang, Jiuxiang Gu, Sai Bi, Yang Zhou, Difan Liu, Feng Liu, Kalyan Sunkavalli, Trung Bui, and Hao Tan. Lrm: Large reconstruction model for single image to 3d. In *Proc. ICLR*, 2024. 2, 3
- [36] Jingwei Huang, Hao Su, and Leonidas Guibas. Robust watertight manifold surface generation method for shapenet models. *arXiv preprint arXiv:1802.01698*, 2018. 7
- [37] Ajay Jain, Ben Mildenhall, Jonathan T Barron, Pieter Abbeel, and Ben Poole. Zero-shot text-guided object generation with dream fields. In *Proc. CVPR*, pages 867–876, 2022. 2, 3
- [38] Haian Jin, Isabella Liu, Peijia Xu, Xiaoshuai Zhang, Songfang Han, Sai Bi, Xiaowei Zhou, Zexiang Xu, and Hao Su. Tensoir: Tensorial inverse rendering. In *Proc. CVPR*, pages 165–174, 2023. 4
- [39] Tao Ju, Frank Losasso, Scott Schaefer, and Joe Warren. Dual contouring of hermite data. In *Proc. SIGGRAPH*, pages 339–346, 2002. 4
- [40] Hiroharu Kato, Yoshitaka Ushiku, and Tatsuya Harada. Neural 3d mesh renderer. In *Proc. CVPR*, pages 3907–3916, 2018. 4
- [41] Bingxin Ke, Anton Obukhov, Shengyu Huang, Nando Metzger, Rodrigo Caye Daudt, and Konrad Schindler. Repurposing diffusion-based image generators for monocular depth estimation. In *Proc. CVPR*, pages 9492–9502, 2024. 2
- [42] Bernhard Kerbl, Georgios Kopanas, Thomas Leimkühler, and George Drettakis. 3d gaussian splatting for real-time radiance field rendering. *ACM Trans. Graph.*, 42(4):139–1, 2023. 3
- [43] Samuli Laine, Janne Hellsten, Tero Karras, Yeongho Seol, Jaakko Lehtinen, and Timo Aila. Modular primitives for high-performance differentiable rendering. *ACM Trans. Graph.*, 39(6):1–14, 2020. 3, 7
- [44] Yushi Lan, Fangzhou Hong, Shuai Yang, Shangchen Zhou, Xuyi Meng, Bo Dai, Xingang Pan, and Chen Change Loy. Ln3diff: Scalable latent neural fields diffusion for speedy 3d generation. In *Proc. ECCV*, pages 112–130, 2024. 3
- [45] Hsin-Ying Lee, Hung-Yu Tseng, and Ming-Hsuan Yang. Exploiting diffusion prior for generalizable dense prediction. In *Proc. CVPR*, pages 7861–7871, 2024. 2
- [46] Jiahao Li, Hao Tan, Kai Zhang, Zexiang Xu, Fujun Luan, Yinghao Xu, Yicong Hong, Kalyan Sunkavalli, Greg Shakhnarovich, and Sai Bi. Instant3d: Fast text-to-3d with sparse-view generation and large reconstruction model. In *Proc. ICLR*, 2024. 3
- [47] Peng Li, Yuan Liu, Xiaoxiao Long, Feihu Zhang, Cheng Lin, Mengfei Li, Xingqun Qi, Shanghang Zhang, Wei Xue, Wenhan Luo, Ping Tan, Wenping Wang, Qifeng Liu, and Yike Guo. Era3d: High-resolution multiview diffusion using efficient row-wise attention. In *Proc. NeurIPS*, 2024. 3
- [48] Ruihui Li, Xianzhi Li, Pheng-Ann Heng, and Chi-Wing Fu. Point cloud upsampling via disentangled refinement. In *Proc. CVPR*, pages 344–353, 2021. 4
- [49] Weiyu Li, Rui Chen, Xuelin Chen, and Ping Tan. Sweetdreamer: Aligning geometric priors in 2d diffusion for consistent text-to-3d. In *Proc. ICLR*, 2024. 3
- [50] Weiyu Li, Jiarui Liu, Rui Chen, Yixun Liang, Xuelin Chen, Ping Tan, and Xiaoxiao Long. Craftsman: High-fidelity mesh generation with 3d native generation and interactive geometry refiner. *arXiv preprint arXiv:2405.14979*, 2024. 3, 8
- [51] Xiaoyu Li, Qi Zhang, Di Kang, Weihao Cheng, Yiming Gao, Jingbo Zhang, Zhihao Liang, Jing Liao, Yan-Pei Cao, and Ying Shan. Advances in 3d generation: A survey. *arXiv preprint arXiv:2401.17807*, 2024. 2, 3
- [52] Yiyi Liao, Simon Donne, and Andreas Geiger. Deep marching cubes: Learning explicit surface representations. In *Proc. CVPR*, pages 2916–2925, 2018. 4
- [53] Chen-Hsuan Lin, Jun Gao, Luming Tang, Towaki Takikawa, Xiaohui Zeng, Xun Huang, Karsten Kreis, Sanja Fidler, Ming-Yu Liu, and Tsung-Yi Lin. Magic3d: High-resolution text-to-3d content creation. In *Proc. CVPR*, pages 300–309, 2023. 3
- [54] Jian Liu, Xiaoshui Huang, Tianyu Huang, Lu Chen, Yue-nan Hou, Shixiang Tang, Ziwei Liu, Wanli Ouyang, Wang-meng Zuo, Junjun Jiang, et al. A comprehensive survey on 3d content generation. *arXiv preprint arXiv:2402.01166*, 2024. 3
- [55] Minghua Liu, Chao Xu, Haian Jin, Linghao Chen, Mukund Varma T, Zexiang Xu, and Hao Su. One-2-3-45: Any single image to 3d mesh in 45 seconds without per-shape optimization. In *Proc. NeurIPS*, pages 22226–22246, 2023. 3

- [56] Ruoshi Liu, Rundi Wu, Basile Van Hoorick, Pavel Tokmakov, Sergey Zakharov, and Carl Vondrick. Zero-1-to-3: Zero-shot one image to 3d object. In *Proc. ICCV*, pages 9298–9309, 2023. 3
- [57] Shichen Liu, Tianye Li, Weikai Chen, and Hao Li. Soft rasterizer: A differentiable renderer for image-based 3d reasoning. In *Proc. ICCV*, pages 7708–7717, 2019. 4
- [58] Yuan Liu, Cheng Lin, Zijiao Zeng, Xiaoxiao Long, Lingjie Liu, Taku Komura, and Wenping Wang. Syncdreamer: Generating multiview-consistent images from a single-view image. In *Proc. ICLR*, 2024. 2, 3, 4
- [59] Xiaoxiao Long, Yuan-Chen Guo, Cheng Lin, Yuan Liu, Zhiyang Dou, Lingjie Liu, Yuexin Ma, Song-Hai Zhang, Marc Habermann, Christian Theobalt, et al. Wonder3d: Single image to 3d using cross-domain diffusion. In *Proc. CVPR*, pages 9970–9980, 2024. 2, 3, 4
- [60] Matthew M Loper and Michael J Black. Opendr: An approximate differentiable renderer. In *Proc. ECCV*, pages 154–169, 2014. 4
- [61] William E. Lorensen and Harvey E. Cline. Marching cubes: A high resolution 3d surface construction algorithm. *ACM SIGGRAPH Comput. Graph.*, 21(4):163–169, 1987. 4
- [62] Jonathan Lorraine, Kevin Xie, Xiaohui Zeng, Chen-Hsuan Lin, Towaki Takikawa, Nicholas Sharp, Tsung-Yi Lin, Ming-Yu Liu, Sanja Fidler, and James Lucas. Att3d: Amortized text-to-3d object synthesis. In *Proc. ICCV*, pages 17946–17956, 2023. 3
- [63] Ilya Loshchilov and Frank Hutter. Decoupled weight decay regularization. In *Proc. ICLR*, 2019. 7
- [64] Yuanxun Lu, Jingyang Zhang, Shiwei Li, Tian Fang, David McKinnon, Yanghai Tsin, Long Quan, Xun Cao, and Yao Yao. Direct2. 5: Diverse text-to-3d generation via multi-view 2.5 d diffusion. In *Proc. CVPR*, pages 8744–8753, 2024. 8
- [65] Aihua Mao, Zihui Du, Junhui Hou, Yaqi Duan, Yong-jin Liu, and Ying He. Pu-flow: A point cloud upsampling network with normalizing flows. *IEEE Trans. Vis. Comput. Graph.*, 29(12):4964–4977, 2022. 4
- [66] Luke Melas-Kyriazi, Iro Laina, Christian Rupprecht, and Andrea Vedaldi. Realfusion: 360deg reconstruction of any object from a single image. In *Proc. CVPR*, pages 8446–8455, 2023. 3
- [67] Lars Mescheder, Michael Oechsle, Michael Niemeyer, Sebastian Nowozin, and Andreas Geiger. Occupancy networks: Learning 3d reconstruction in function space. In *Proc. CVPR*, pages 4460–4470, 2019. 4
- [68] Gal Metzer, Elad Richardson, Or Patashnik, Raja Giryes, and Daniel Cohen-Or. Latent-nerf for shape-guided generation of 3d shapes and textures. In *Proc. CVPR*, pages 12663–12673, 2023. 3
- [69] Oscar Michel, Roi Bar-On, Richard Liu, Sagie Benaim, and Rana Hanocka. Text2mesh: Text-driven neural stylization for meshes. In *Proc. CVPR*, pages 13492–13502, 2022. 3
- [70] Ben Mildenhall, Pratul P. Srinivasan, Matthew Tancik, Jonathan T. Barron, Ravi Ramamoorthi, and Ren Ng. Nerf: Representing scenes as neural radiance fields for view synthesis. In *Proc. ECCV*, pages 405–421, 2020. 3
- [71] Nasir Mohammad Khalid, Tianhao Xie, Eugene Belilovsky, and Tiberiu Popa. Clip-mesh: Generating textured meshes from text using pretrained image-text models. In *Proc. SIGGRAPH Asia*, pages 1–8, 2022. 3
- [72] Jacob Munkberg, Jon Hasselgren, Tianchang Shen, Jun Gao, Wenzheng Chen, Alex Evans, Thomas Müller, and Sanja Fidler. Extracting triangular 3d models, materials, and lighting from images. In *Proc. CVPR*, pages 8280–8290, 2022. 3
- [73] Baptiste Nicolet, Alec Jacobson, and Wenzel Jakob. Large steps in inverse rendering of geometry. *ACM Trans. Graph.*, 40(6):1–13, 2021. 4
- [74] Gregory M Nielson. Dual marching cubes. In *IEEE visualization 2004*, pages 489–496, 2004. 4, 6
- [75] Maxime Oquab, Timothée Darcet, Théo Moutakanni, Huy V. Vo, Marc Szafraniec, Vasil Khalidov, Pierre Fernandez, Daniel HAZIZA, Francisco Massa, Alaaeldin El-Nouby, Mido Assran, Nicolas Ballas, Wojciech Galuba, Russell Howes, Po-Yao Huang, Shang-Wen Li, Ishan Misra, Michael Rabbat, Vasu Sharma, Gabriel Synnaeve, Hu Xu, Herve Jegou, Julien Mairal, Patrick Labatut, Armand Joulin, and Piotr Bojanowski. Dinov2: Learning robust visual features without supervision. *Trans. Mach. Learn. Res.*, 2024. 5
- [76] Werner Palfinger. Continuous remeshing for inverse rendering. *Comput. Animat. Virtual Worlds*, 33(5):e2101, 2022. 4, 5, 7, 8
- [77] Jeong Joon Park, Peter Florence, Julian Straub, Richard Newcombe, and Steven Lovegrove. DeepSDF: Learning continuous signed distance functions for shape representation. In *Proc. CVPR*, pages 165–174, 2019. 4
- [78] Ben Poole, Ajay Jain, Jonathan T. Barron, and Ben Mildenhall. DreamFusion: Text-to-3d using 2d diffusion. In *Proc. ICLR*, 2023. 2, 3
- [79] Guocheng Qian, Abdullellah Abualshour, Guohao Li, Ali Thabet, and Bernard Ghanem. Pu-gcn: Point cloud upsampling using graph convolutional networks. In *Proc. CVPR*, pages 11683–11692, 2021. 4
- [80] Guocheng Qian, Jinjie Mai, Abdullah Hamdi, Jian Ren, Aliaksandr Siarohin, Bing Li, Hsin-Ying Lee, Ivan Skokhodov, Peter Wonka, Sergey Tulyakov, and Bernard Ghanem. Magic123: One image to high-quality 3d object generation using both 2d and 3d diffusion priors. In *Proc. ICLR*, 2024. 3
- [81] Yue Qian, Junhui Hou, Sam Kwong, and Ying He. Pugeonet: A geometry-centric network for 3d point cloud upsampling. In *Proc. ECCV*, pages 752–769, 2020. 2, 4
- [82] Yue Qian, Junhui Hou, Sam Kwong, and Ying He. Deep magnification-flexible upsampling over 3d point clouds. *IEEE Trans. Image Process.*, 30:8354–8367, 2021. 4
- [83] Lingteng Qiu, Guanying Chen, Xiaodong Gu, Qi Zuo, Mutian Xu, Yushuang Wu, Weihao Yuan, Zilong Dong, Liefeng Bo, and Xiaoguang Han. Richdreamer: A generalizable normal-depth diffusion model for detail richness in text-to-3d. In *Proc. CVPR*, pages 9914–9925, 2024. 3
- [84] Alec Radford, Jong Wook Kim, Chris Hallacy, Aditya Ramesh, Gabriel Goh, Sandhini Agarwal, Girish Sastry,

- Amanda Asbell, Pamela Mishkin, Jack Clark, et al. Learning transferable visual models from natural language supervision. In *Proc. ICML*, pages 8748–8763, 2021. 2, 3
- [85] Amit Raj, Srinivas Kaza, Ben Poole, Michael Niemeyer, Nataniel Ruiz, Ben Mildenhall, Shiran Zada, Kfir Aberman, Michael Rubinstein, Jonathan Barron, et al. Dreambooth3d: Subject-driven text-to-3d generation. In *Proc. ICCV*, pages 2349–2359, 2023. 2, 3
- [86] Edoardo Remelli, Artem Lukoianov, Stephan Richter, Benoit Guillard, Timur Bagautdinov, Pierre Baque, and Pascal Fua. Meshsdf: Differentiable iso-surface extraction. In *Proc. NeurIPS*, pages 22468–22478, 2020. 4
- [87] Robin Rombach, Andreas Blattmann, Dominik Lorenz, Patrick Esser, and Björn Ommer. High-resolution image synthesis with latent diffusion models. In *Proc. CVPR*, pages 10684–10695, 2022. 2, 3, 4, 7
- [88] Tim Salimans and Jonathan Ho. Progressive distillation for fast sampling of diffusion models. In *Proc. ICLR*, 2022. 5
- [89] Tianchang Shen, Jun Gao, Kangxue Yin, Ming-Yu Liu, and Sanja Fidler. Deep marching tetrahedra: a hybrid representation for high-resolution 3d shape synthesis. In *Proc. NeurIPS*, pages 6087–6101, 2021. 4
- [90] Tianchang Shen, Jacob Munkberg, Jon Hasselgren, Kangxue Yin, Zian Wang, Wenzheng Chen, Zan Gojcic, Sanja Fidler, Nicholas Sharp, and Jun Gao. Flexible isosurface extraction for gradient-based mesh optimization. *ACM Trans. Graph.*, 42(4):37–1, 2023. 4, 5, 8
- [91] Ruoxi Shi, Hansheng Chen, Zhuoyang Zhang, Minghua Liu, Chao Xu, Xinyue Wei, Linghao Chen, Chong Zeng, and Hao Su. Zero123++: a single image to consistent multi-view diffusion base model. *arXiv preprint arXiv:2310.15110*, 2023. 3, 4
- [92] Yichun Shi, Peng Wang, Jianglong Ye, Long Mai, Kejie Li, and Xiao Yang. Mvdream: Multi-view diffusion for 3d generation. In *Proc. ICLR*, 2024. 3
- [93] Zifan Shi, Sida Peng, Yinghao Xu, Andreas Geiger, Yiyi Liao, and Yujun Shen. Deep generative models on 3d representations: A survey. *arXiv preprint arXiv:2210.15663*, 2022. 3
- [94] Yawar Siddiqui, Antonio Alliegro, Alexey Artemov, Tatiana Tommasi, Daniele Sirigatti, Vladislav Rosov, Angela Dai, and Matthias Nießner. Meshgpt: Generating triangle meshes with decoder-only transformers. In *Proc. CVPR*, pages 19615–19625, 2024. 3
- [95] Jiaming Song, Chenlin Meng, and Stefano Ermon. Denoising diffusion implicit models. In *Proc. ICLR*, 2021. 3
- [96] Pratul P Srinivasan, Boyang Deng, Xiuming Zhang, Matthew Tancik, Ben Mildenhall, and Jonathan T Barron. Nerv: Neural reflectance and visibility fields for relighting and view synthesis. In *Proc. CVPR*, pages 7495–7504, 2021. 4
- [97] Jingxiang Sun, Bo Zhang, Ruizhi Shao, Lizhen Wang, Wen Liu, Zhenda Xie, and Yebin Liu. Dreamcraft3d: Hierarchical 3d generation with bootstrapped diffusion prior. In *Proc. ICLR*, 2024. 3
- [98] Junshu Tang, Tengfei Wang, Bo Zhang, Ting Zhang, Ran Yi, Lizhuang Ma, and Dong Chen. Make-it-3d: High-fidelity 3d creation from a single image with diffusion prior. In *Proc. ICCV*, pages 22819–22829, 2023. 3
- [99] Jiayang Tang, Zhaoxi Chen, Xiaokang Chen, Tengfei Wang, Gang Zeng, and Ziwei Liu. Lgm: Large multi-view gaussian model for high-resolution 3d content creation. In *Proc. ECCV*, pages 1–18, 2024. 3
- [100] Jiayang Tang, Jiawei Ren, Hang Zhou, Ziwei Liu, and Gang Zeng. Dreamgaussian: Generative gaussian splatting for efficient 3d content creation. In *Proc. ICLR*, 2024. 3
- [101] Jiayang Tang, Zhaoshuo Li, Zekun Hao, Xian Liu, Gang Zeng, Ming-Yu Liu, and Qingsheng Zhang. Edgerunner: Auto-regressive auto-encoder for artistic mesh generation. In *Proc. ICLR*, 2025. 3
- [102] Gabriel Taubin. A signal processing approach to fair surface design. In *Proc. SIGGRAPH*, pages 351–358, 1995. 7
- [103] Dmitry Tochilkin, David Pankratz, Zexiang Liu, Zixuan Huang, Adam Letts, Yangguang Li, Ding Liang, Christian Laforte, Varun Jampani, and Yan-Pei Cao. Tripotr: Fast 3d object reconstruction from a single image. *arXiv preprint arXiv:2403.02151*, 2024. 3
- [104] Shimon Vainer, Mark Boss, Mathias Parger, Konstantin Kutsy, Dante De Nigris, Ciara Rowles, Nicolas Perony, and Simon Donn . Collaborative control for geometry-conditioned pbr image generation. In *Proc. ECCV*, pages 127–145, 2024. 2, 4
- [105] Haochen Wang, Xiaodan Du, Jiahao Li, Raymond A Yeh, and Greg Shakhnarovich. Score jacobian chaining: Lifting pretrained 2d diffusion models for 3d generation. In *Proc. CVPR*, pages 12619–12629, 2023. 3
- [106] Nanyang Wang, Yinda Zhang, Zhuwen Li, Yanwei Fu, Wei Liu, and Yu-Gang Jiang. Pixel2mesh: Generating 3d mesh models from single rgb images. In *Proc. ECCV*, pages 52–67, 2018. 4
- [107] Yitong Wang, Xudong Xu, Li Ma, Haoran Wang, and Bo Dai. Boosting 3d object generation through pbr materials. In *Proc. SIGGRAPH Asia*, pages 1–11, 2024. 2, 4, 8
- [108] Yufei Wang, Wenhan Yang, Xinyuan Chen, Yaohui Wang, Lanqing Guo, Lap-Pui Chau, Ziwei Liu, Yu Qiao, Alex C Kot, and Bihan Wen. Sinsr: diffusion-based image super-resolution in a single step. In *Proc. CVPR*, pages 25796–25805, 2024. 2
- [109] Zhihao Wang, Jian Chen, and Steven CH Hoi. Deep learning for image super-resolution: A survey. *IEEE Trans. Pattern Anal. Mach. Intell.*, 43(10):3365–3387, 2020. 4
- [110] Zhengyi Wang, Cheng Lu, Yikai Wang, Fan Bao, Chongxuan Li, Hang Su, and Jun Zhu. Prolificdreamer: High-fidelity and diverse text-to-3d generation with variational score distillation. In *Proc. NeurIPS*, pages 8406–8441, 2024. 3
- [111] Zhengyi Wang, Yikai Wang, Yifei Chen, Chendong Xiang, Shuo Chen, Dajiang Yu, Chongxuan Li, Hang Su, and Jun Zhu. Crm: Single image to 3d textured mesh with convolutional reconstruction model. In *Proc. ECCV*, pages 57–74, 2024. 3
- [112] Haohan Weng, Yikai Wang, Tong Zhang, C. L. Philip Chen, and Jun Zhu. Pivotmesh: Generic 3d mesh generation via pivot vertices guidance. In *Proc. ICLR*, 2025. 3

- [113] Kailu Wu, Fangfu Liu, Zhihan Cai, Runjie Yan, Hanyang Wang, Yating Hu, Yueqi Duan, and Kaisheng Ma. Unique3d: High-quality and efficient 3d mesh generation from a single image. In *Proc. NeurIPS*, 2024. [2](#), [3](#), [4](#), [6](#), [7](#), [8](#)
- [114] Shuang Wu, Youtian Lin, Feihu Zhang, Yifei Zeng, Jingxi Xu, Philip Torr, Xun Cao, and Yao Yao. Direct3d: Scalable image-to-3d generation via 3d latent diffusion transformer. *arXiv preprint arXiv:2405.14832*, 2024. [3](#)
- [115] Zhirong Wu, Shuran Song, Aditya Khosla, Fisher Yu, Linguang Zhang, Xiaoou Tang, and Jianxiong Xiao. 3d shapenets: A deep representation for volumetric shapes. In *Proc. CVPR*, pages 1912–1920, 2015. [3](#)
- [116] Guangkai Xu, Yongtao Ge, Mingyu Liu, Chengxiang Fan, Kangyang Xie, Zhiyue Zhao, Hao Chen, and Chunhua Shen. What matters when repurposing diffusion models for general dense perception tasks? In *Proc. ICLR*, 2025. [2](#)
- [117] Jiale Xu, Weihao Cheng, Yiming Gao, Xintao Wang, Shenghua Gao, and Ying Shan. Instantmesh: Efficient 3d mesh generation from a single image with sparse-view large reconstruction models. *arXiv preprint arXiv:2404.07191*, 2024. [2](#), [3](#), [6](#), [7](#)
- [118] Xingguang Yan, Han-Hung Lee, Ziyu Wan, and Angel X Chang. An object is worth 64x64 pixels: Generating 3d object via image diffusion. In *Proc. 3DV*, 2024. [3](#)
- [119] Chongjie Ye, Lingteng Qiu, Xiaodong Gu, Qi Zuo, Yushuang Wu, Zilong Dong, Liefeng Bo, Yuliang Xiu, and Xiaoguang Han. Stablenormal: Reducing diffusion variance for stable and sharp normal. *ACM Trans. Graph.*, 43(6):1–18, 2024. [7](#), [8](#)
- [120] Taoran Yi, Jiemin Fang, Junjie Wang, Guanjun Wu, Lingxi Xie, Xiaopeng Zhang, Wenyu Liu, Qi Tian, and Xinggang Wang. Gaussiandreamer: Fast generation from text to 3d gaussians by bridging 2d and 3d diffusion models. In *CVPR*, pages 6796–6807, 2024. [3](#)
- [121] Wang Yifan, Shihao Wu, Hui Huang, Daniel Cohen-Or, and Olga Sorkine-Hornung. Patch-based progressive 3d point set upsampling. In *Proc. CVPR*, pages 5958–5967, 2019. [4](#)
- [122] Kim Youwang, Tae-Hyun Oh, and Gerard Pons-Moll. Paint-it: Text-to-texture synthesis via deep convolutional texture map optimization and physically-based rendering. In *Proc. CVPR*, pages 4347–4356, 2024. [4](#)
- [123] Lequan Yu, Xianzhi Li, Chi-Wing Fu, Daniel Cohen-Or, and Pheng-Ann Heng. Pu-net: Point cloud upsampling network. In *Proc. CVPR*, pages 2790–2799, 2018. [2](#), [4](#)
- [124] Zongsheng Yue, Jianyi Wang, and Chen Change Loy. Resshift: Efficient diffusion model for image super-resolution by residual shifting. In *Proc. NeurIPS*, pages 13294–13307, 2023. [2](#)
- [125] Biao Zhang, Jiapeng Tang, Matthias Niessner, and Peter Wonka. 3dshape2vecset: A 3d shape representation for neural fields and generative diffusion models. *ACM Trans. Graph.*, 42(4):1–16, 2023. [3](#)
- [126] Kai Zhang, Fujun Luan, Zhengqi Li, and Noah Snavely. Iron: Inverse rendering by optimizing neural sdfs and materials from photometric images. In *Proc. CVPR*, pages 5565–5574, 2022. [4](#)
- [127] Longwen Zhang, Ziyu Wang, Qixuan Zhang, Qiwei Qiu, Anqi Pang, Haoran Jiang, Wei Yang, Lan Xu, and Jingyi Yu. Clay: A controllable large-scale generative model for creating high-quality 3d assets. *ACM Trans. Graph.*, 43(4):1–20, 2024. [2](#), [3](#), [6](#), [7](#)
- [128] Qijian Zhang, Junhui Hou, Yue Qian, Antoni B Chan, Juyong Zhang, and Ying He. Reggeonet: Learning regular representations for large-scale 3d point clouds. *Int. J. Comput. Vis.*, 130(12):3100–3122, 2022. [3](#)
- [129] Qijian Zhang, Junhui Hou, Yue Qian, Yiming Zeng, Juyong Zhang, and Ying He. Flattening-net: Deep regular 2d representation for 3d point cloud analysis. *IEEE Trans. Pattern Anal. Mach. Intell.*, 45(8):9726–9742, 2023. [3](#), [4](#)
- [130] Xiuming Zhang, Pratul P Srinivasan, Boyang Deng, Paul Debevec, William T Freeman, and Jonathan T Barron. Nerfactor: Neural factorization of shape and reflectance under an unknown illumination. *ACM Trans. Graph.*, 40(6):1–18, 2021. [4](#)